ISIJ International, Vol. 62 (2022), No. 1, pp. 12–19
https://doi.org/10.2355/isijinternational.ISIJINT-2021-267

Aluminum Deoxidation Equilibrium in Molten Fe–Co Alloys

Jonah GAMUTAN,[1)]* Kosei AKAISHI,[1)] Takahiro SATO[2)] and Takahiro MIKI[1)]

1) Department of Metallurgy, Materials Science and Materials Processing, Graduate School of Engineering, Tohoku University, Aobayama 6-6-02, Sendai, 980-8579 Japan.
2) Institute for Multidisciplinary Materials Science, Department of Metallurgy, Materials Science and Materials Processing, Graduate School of Engineering, Tohoku University, Katahira 2-1-1, Sendai, 980-8577 Japan.

(*Received on June 14, 2021; accepted on September 2, 2021*)

Aluminum deoxidation equilibrium of molten Fe–Co alloy was experimentally measured using a chemical equilibrium method and numerically assessed using a sub-regular solution model based on Darken's quadratic formalism and a Redlich-Kister type polynomial at 1 873 K. It was found that the degree of oxygen content reduction by Al-deoxidation decreased with increasing cobalt concentration in the alloy, peaking at around 40 to 60 mass% Co, and then improved with further increase in cobalt concentration. The following binary interaction parameters between cobalt and aluminum were derived in this study:

$$^{0}\Omega_{Co-Al} = -387\,360\,[J/mol],\ ^{1}\Omega_{Co-Al} = 309\,420\,[J/mol]$$

It was also found that the above binary interaction parameters can accurately determine Al-deoxidation equilibrium of pure liquid cobalt. Finally, the critical point at which Al_2O_3 and $CoO{\cdot}Al_2O_3$ coexist throughout the whole composition range of the alloy was also estimated from the experimental results in this study.

KEY WORDS: Al-deoxidation equilibrium; Fe–Co alloys; quadratic formalism; Redlich-Kister polynomial.

1. Introduction

Recently, there has been an increasing demand for alloys belonging to the Fe–Co system for use in modern industrial applications due to their excellent magnetic properties and good mechanical strength. In particular, Fe–Co alloys exhibit the highest saturation magnetization of ferromagnetic materials and possess the ability to function as either soft or hard magnets by simple changes in composition. Hence, they are widely used as magnetic materials in the development of motors and generators for aerospace and power applications.[1)] However, under the presence of oxygen, performance properties of these alloys were found to deteriorate due to a decrease in their magnetic permeability and increase in the coercive force.[2)]

In addition, Fe–Co steels alloyed with Ni, commonly referred to as maraging steels, also exhibit excellent strength and toughness without loss of ductility, making them good structural materials for aerospace applications such as landing gears and fuel rocket chambers. Due to the high safety requirements in these applications, it is therefore important to control the metal composition such that formation of defects is prevented. This is achieved by deoxidation during secondary refining in the steelmaking process so as to minimize oxygen concentration in the alloy prior to solidification and inhibit the formation of blowholes and oxide inclusions.

From the above, controlling oxygen content in the Fe–Co and Fe–Ni–Co alloys by deoxidation is therefore necessary to produce high-quality magnetic and structural materials. Deoxidation is usually accomplished by the addition of elements with higher affinity for oxygen than iron to form oxides that are readily removed from the molten alloy. In the steelmaking process, one of the most commonly used deoxidizing agents is aluminum due to its strong affinity with oxygen. Understanding the thermodynamic relationship between aluminum and oxygen in molten Fe–Co and Fe–Ni–Co alloys is therefore necessary to estimate the extent of oxygen content reduction by Al-deoxidation such that the magnetic and structural properties of these alloys are maintained. Although Al-deoxidation equilibrium in the molten Fe–Ni alloy system has already been extensively investigated,[3–11)] Al-deoxidation equilibrium in the molten Fe–Co alloy has been reported by Aleksandrov & Dashevskii only.[2)] Through a thermodynamic assessment, their results indicated that with increasing cobalt content in the melt, the Al-deoxidation efficiency increases and the minimum oxygen solubility shifts to lower aluminum contents. However, since their results were based on a number of assumptions due to lack of experimental and reference data, further experimental investigation is necessary.

Moreover, Al-deoxidation equilibrium in pure liquid cobalt has been reported by Ishihara *et al.* only. Using an Al_2O_3 cru-

* Corresponding author: E-mail: jonah.gamutan@gmail.com

cible, they were able to measure Al-deoxidation equilibrium in liquid cobalt from 1 873 to 1 973 K and determine the temperature dependence of Al_2O_3 formation within this temperature range.[12] However, it is worth noting that although Al_2O_3 normally forms as the deoxidation product during Al-deoxidation, cobalt aluminate ($CoO{\cdot}Al_2O_3$) formation is also possible at high oxygen and low aluminum additions.

Therefore, given the importance of obtaining high-quality Fe–Co based alloys, Al-deoxidation equilibrium in molten Fe–Co alloys coexisting with Al_2O_3 or $CoO{\cdot}Al_2O_3$ at 1 873 K was investigated in this study. Al-deoxidation experiments were carried out in molten Fe– 10, 20, 30, 40, 60, and 80 mass% Co samples. Thermodynamic assessment was then conducted using a sub-regular solution model based on Darken's quadratic formalism[13] and a Redlich-Kister type polynomial[14,15] using the present experimental data and reference values. Details of the analysis employed in this study have already been explained in several papers[16–20] and have been found to be appropriate in calculating the deoxidation equilibrium, particularly in high alloy systems.

2. Experimental Method

2.1. Al-deoxidation Experiments

In this study, Al-deoxidation experiments were carried out in a high-frequency induction furnace (MU-1700D, Sekisui Chemical Co., Ltd.) at 1 873 K as shown in **Fig. 1**. The reaction tube (68 × 50 × 500 mm.) was made of transparent quartz and the actual temperature was measured using a radiation thermometer (FTK9S, Japan Sensor Co., Ltd.). The emissivity of the radiation thermometer was calibrated by comparing the liquidus temperature of the alloy taken from the Fe–Co alloy phase diagram[21] and the temperature at which the first solid phase appeared during cooling from 1 873 K.

About 25 grams of Fe–Co alloy at varying compositions

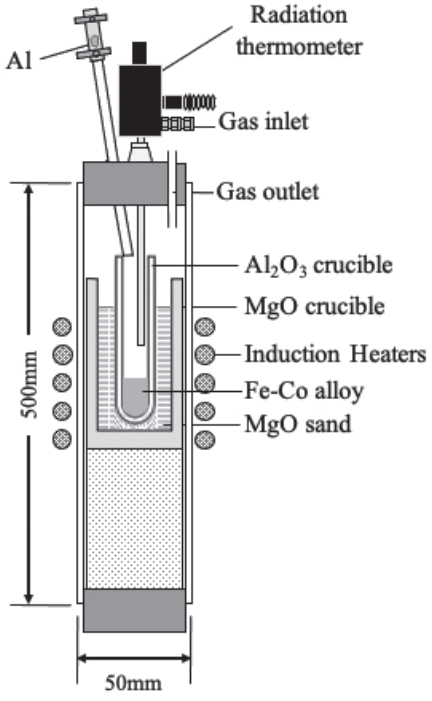

Fig. 1. Al-deoxidation experiment set-up.

(10, 20, 30, 40, 60, and 80 mass% Co) were prepared from reagent grade electrolytic iron (99.9% purity), and electrolytic cobalt (99.9% purity). Granular Fe_3O_4 (99.5% purity) was used as the source of oxygen while pure aluminum (99.99% purity) was used as the deoxidizing agent. For the heating experiments, the samples were placed in an inner Al_2O_3 crucible (21 × 17 × 100 mm.) fitted into a protective outer MgO crucible (40 × 30 × 100 mm.) filled with MgO sand to prevent thermal spalling.

First, electrolytic iron, electrolytic cobalt, and granular Fe_3O_4 were weighed according to the target compositions and then placed inside the furnace with Ar gas flowing at a high flowrate of 2.0 L $min.^{-1}$ to completely replace the air inside the reaction tube. After 20 minutes, Ar gas flow was reduced to 1.0 L $min.^{-1}$ and the temperature was gradually raised to melt the sample. When the temperature stabilized at the steelmaking temperature of 1 873 K and complete melting of the sample was confirmed, aluminum was added through the injection pipe. The temperature was held at 1 873 K for another 50 minutes based on our preliminary deoxidation experiments where it was confirmed that 40 minutes of holding time was enough to reach equilibrium. Finally, the power of the furnace was turned off and the sample was cooled to room temperature by quenching with Ar gas.

2.2. Characterization of the Samples

After removing the shrinkage cavity, the chemical composition of the obtained equilibrium samples was determined using the following methods. First, cobalt and aluminum concentrations of the alloy were determined using an Inductively Coupled Plasma Emission Spectrometer (ICPS-8100, Shimadzu Corp.) by dissolving about 0.5–1.5 grams of the sample in an aqua regia solution prepared by mixing 3-parts concentrated HCl to 1-part concentrated HNO_3. For samples with high cobalt concentrations, dissolution in concentrated HNO_3 was enough.

Next, oxygen concentration was determined using an inert gas fusion technique (LECO-ONH836 Element Analyzer). About 0.5–1.0 grams of the alloy were cut using a fine cutter and then polished using SiC paper up to #600 with ultrasonic cleaning in ethanol solution after every step. Finally, the polished samples were kept in an anhydrous ethanol solution until analysis to prevent oxygen adsorption on the sample surface. Due to the pinch effect caused by induction heating, the measured oxygen content using this method is expected to correspond to the dissolved oxygen concentration in the metal phase. Meanwhile, iron content of the equilibrium samples was taken as the remainder of the measured cobalt, aluminum and oxygen values.

The interface between the alloy and the crucible was observed using SEM-EDS (JEOL JSM-6510 and Oxford INCA Energy 250XT) by hot-mounting the Al_2O_3 crucible in a carbon filler resin. Elemental mapping and point analysis of the metal-crucible interface were carried out at an acceleration voltage (AV) of 15 kV, a working distance (WD) of 15 mm and a spot size (SS) of 60 nm.

3. Results and Discussion

3.1. Al-deoxidation in Molten Fe–Co Alloys

The metal phase composition and the oxide phase in

equilibrium with Fe – 10, 20, 30, 40, 60, and 80 mass% Co samples at 1 873 K are shown in **Table 1**. The oxide phase in equilibrium with the melt was found to be Al_2O_3 with negligible FeO content for almost all samples. The FeO content in the oxide phase was confirmed to be low enough such that the activity of Al_2O_3 can be assumed as unity in the numerical assessment, which will be discussed in detail in the following section. However, in Sample 26, a blue-colored layer was instead generated on the metal-crucible interface, suggesting the formation of a different oxide phase. SEM-EDS mapping and point analysis of this layer indicated the formation of cobalt aluminate ($CoO{\cdot}Al_2O_3$). The details of this analysis will be further discussed later in Section 3.3.

Table 1. Metal phase composition and the oxide phase in equilibrium with molten Fe–Co alloys at 1 873 K.

Sample No.	Composition, (mass%)			Equilibrium Oxide
	[Co]	[Al]	[O]	
Fe-10 mass% Co				
1	10.581	0.001	0.065	Al_2O_3
2	10.156	0.001	0.038	Al_2O_3
Fe-20 mass% Co				
3	20.154	0.515	0.030	Al_2O_3
4	20.269	0.384	0.011	Al_2O_3
5	19.968	0.180	0.025	Al_2O_3
6	20.055	0.001	0.029	Al_2O_3
7	20.106	0.385	0.025	Al_2O_3
8	20.209	0.000	0.035	Al_2O_3
9	20.423	0.062	0.028	Al_2O_3
10	20.351	0.106	0.020	Al_2O_3
Fe-30 mass% Co				
11	32.308	0.265	0.013	Al_2O_3
12	31.681	0.086	0.023	Al_2O_3
13	32.948	0.091	0.006	Al_2O_3
14	32.556	0.015	0.008	Al_2O_3
15	31.675	0.004	0.061	Al_2O_3
16	32.163	0.004	0.069	Al_2O_3
Fe-40 mass% Co				
17	41.744	0.088	0.006	Al_2O_3
18	39.910	0.087	0.098	Al_2O_3
19	39.928	0.380	0.012	Al_2O_3
20	39.912	0.624	0.021	Al_2O_3
Fe-60 mass% Co				
21	59.926	0.055	0.113	Al_2O_3
22	60.278	0.062	0.034	Al_2O_3
23	59.407	0.128	0.018	Al_2O_3
24	58.963	0.252	0.041	Al_2O_3
25	59.668	0.378	0.023	Al_2O_3
Fe-80 mass% Co				
26	80.005	0.029	0.086	$CoO{\cdot}Al_2O_3$
27	80.130	0.031	0.017	Al_2O_3
28	80.009	0.074	0.062	Al_2O_3
29	80.404	0.205	0.014	Al_2O_3
30	79.710	0.304	0.015	Al_2O_3

3.2. Numerical Assessment of Al-deoxidation

As previously mentioned, a sub-regular solution model with Redlich-Kister type polynomial was used to numerically assess Al-deoxidation equilibrium in molten Fe–Co alloys. Although Wagner's formalism is one of the most common models used, it is essentially available only for dilute solutions and many difficulties have been associated with its application to high alloy steels. In the current model, for the condensed phases, the pure substance was set as the standard state (Raoultian standard state) while for oxygen, the oxygen dissolved in the melt equilibrating with 101 325 Pa (1 atm) of oxygen gas was set as the standard state. In this case, the oxygen dissolution reaction can be expressed as Eq. (1) and the Gibbs free energy change is equal to zero such that Eq. (3) holds.

$$2\underline{O} = O_2(g) \quad \cdots\cdots (1)$$

$$\Delta G^\circ = -RT\ln K = 0 \quad \cdots\cdots (2)$$

$$a_O = \left(P_{O_2} / P^0\right)^{1/2} \quad \cdots\cdots (3)$$

where, R is the gas constant (8.3145 J/mol·K), T is the absolute temperature, K is the equilibrium constant, a_O is the activity of oxygen, P_{O_2} is the partial pressure of oxygen gas in Pa and P^0 is the standard pressure in Pa. From this, the activity or the partial pressure of oxygen at equilibrium is hence independent of the kind of metal solvent.

Meanwhile, Al-deoxidation reaction can be expressed as:

$$2[Al] + 3[O] = Al_2O_3(s) \quad \cdots\cdots (4)$$

The above equation can be further separated into the following two equations:

$$2[Al] + \frac{3}{2}O_2(g) = Al_2O_3(s) \quad \cdots\cdots (5)$$

$$3[O] = \frac{3}{2}O_2(g) \quad \cdots\cdots (6)$$

The Gibbs free energy change of Eq. (5) is simply equal to the Gibbs free energy of formation of Al_2O_3 ($\Delta G^\circ_{f,\,Al_2O_3}$) while that of Eq. (6) is zero such that the equilibrium constant, $K_{Al_2O_3}$, can be expressed as follows:

$$\begin{aligned}\ln K_{Al_2O_3} &= -\frac{\Delta G^\circ_{f,\,Al_2O_3}}{RT} \\ &= \ln a_{Al_2O_3} - 2\ln\gamma_{Al} - 3\ln\gamma_O - 2\ln X_{Al} - 3\ln X_O \\ &= -2\ln\gamma_{Al} - 3\ln\gamma_O - 2\ln X_{Al} - 3\ln X_O \\ &\left(\therefore a_{Al_2O_3} = 1\right)\end{aligned} \quad \cdots\cdots (7)$$

Where, a_i, γ_i, and X_i denote the activity, activity coefficient and mole fraction of component i, respectively. As previously mentioned, the activity of Al_2O_3 can be taken as unity, since the deoxidation product is pure solid Al_2O_3, except for Sample 26.

Next, the excess Gibbs free energy change of mixing (ΔG_M^{ex}) in the Fe–Co–Al–O system can be described as in Eq. (8) by using the Redlich-Kister type polynomial.

$$\begin{aligned}\Delta G_M^{ex} = {} & X_{Fe}X_{Co}{}^{\circ}\Omega_{Fe-Co} + X_{Fe}X_{Co}{}^{1}\Omega_{Fe-Co}\left(X_{Fe}-X_{Co}\right)\\ & + X_{Fe}X_{Co}{}^{2}\Omega_{Fe-Co}\left(X_{Fe}-X_{Co}\right)^2\\ & + X_{Fe}X_{Al}{}^{\circ}\Omega_{Fe-Al} + X_{Fe}X_{Al}{}^{1}\Omega_{Fe-Al}\left(X_{Fe}-X_{Al}\right)\\ & + X_{Fe}X_{O}{}^{\circ}\Omega_{Fe-O} + X_{Fe}X_{O}{}^{1}\Omega_{Fe-O}\left(X_{Fe}-X_{O}\right)\\ & + X_{Co}X_{Al}{}^{\circ}\Omega_{Co-Al} + X_{Co}X_{Al}{}^{1}\Omega_{Co-Al}\left(X_{Co}-X_{Al}\right)\\ & + X_{Co}X_{O}{}^{\circ}\Omega_{Co-O} + X_{Co}X_{O}{}^{1}\Omega_{Co-O}\left(X_{Co}-X_{O}\right)\\ & + X_{Al}X_{O}{}^{\circ}\Omega_{Al-O}\end{aligned} \quad \text{..... (8)}$$

where X_i denotes the mole fraction of component i and ${}^{n}\Omega_{i-j}$ denotes the nth order binary interaction parameters of components i-j. From this, the partial molar excess free energy change of cobalt, aluminum, and oxygen can be derived as follows.

$$\begin{aligned}\Delta\bar{G}_{\mathrm{Co}}^{\mathrm{ex}} &= RT\ln\gamma_{\mathrm{Co}}\\ &= \Delta G^{\mathrm{ex}} + \left(1-X_{\mathrm{Co}}\right)\frac{\partial\Delta G^{\mathrm{ex}}}{\partial X_{\mathrm{Co}}} - X_{\mathrm{Al}}\frac{\partial\Delta G^{\mathrm{ex}}}{\partial X_{\mathrm{Al}}} - X_{\mathrm{O}}\frac{\partial\Delta G^{\mathrm{ex}}}{\partial X_{\mathrm{O}}}\\ &= X_{\mathrm{Fe}}\left(1-X_{\mathrm{Co}}\right){}^{0}\Omega_{\mathrm{Fe-Co}}\\ &\quad + X_{\mathrm{Fe}}\left(X_{\mathrm{Fe}}-2X_{\mathrm{Co}}-2X_{\mathrm{Fe}}X_{\mathrm{Co}}+2X_{\mathrm{Co}}^2\right){}^{1}\Omega_{\mathrm{Fe-Co}}\\ &\quad + X_{\mathrm{Fe}}\left(X_{\mathrm{Fe}}-X_{\mathrm{Co}}\right)\left(-X_{\mathrm{Fe}}-X_{\mathrm{Co}}-5X_{\mathrm{Fe}}X_{\mathrm{Co}}+5X_{\mathrm{Co}}^2\right){}^{2}\Omega_{\mathrm{Fe-Co}}\\ &\quad - X_{\mathrm{Fe}}X_{\mathrm{Al}}{}^{0}\Omega_{\mathrm{Fe-Al}} - 2X_{\mathrm{Fe}}X_{\mathrm{Al}}\left(X_{\mathrm{Fe}}-X_{\mathrm{Al}}\right){}^{1}\Omega_{\mathrm{Fe-Al}}\\ &\quad - X_{\mathrm{Fe}}X_{\mathrm{O}}{}^{0}\Omega_{\mathrm{Fe-O}} - 2X_{\mathrm{Fe}}X_{\mathrm{O}}\left(X_{\mathrm{Fe}}-X_{\mathrm{O}}\right){}^{1}\Omega_{\mathrm{Fe-O}}\\ &\quad + X_{\mathrm{Al}}\left(1-X_{\mathrm{Co}}\right){}^{0}\Omega_{\mathrm{Co-Al}}\\ &\quad - X_{\mathrm{Al}}\left(X_{\mathrm{Al}}-2X_{\mathrm{Co}}-2X_{\mathrm{Co}}X_{\mathrm{Al}}+2X_{\mathrm{Co}}^2\right){}^{1}\Omega_{\mathrm{Co-Al}}\\ &\quad + X_{\mathrm{O}}\left(1-X_{\mathrm{Co}}\right){}^{0}\Omega_{\mathrm{Co-O}}\\ &\quad - X_{\mathrm{O}}\left(X_{\mathrm{O}}-2X_{\mathrm{Co}}-2X_{\mathrm{Co}}X_{\mathrm{O}}+2X_{\mathrm{Co}}^2\right){}^{1}\Omega_{\mathrm{Co-O}}\\ &\quad - X_{\mathrm{Al}}X_{\mathrm{O}}{}^{0}\Omega_{\mathrm{Al-O}}\end{aligned} \quad \text{..... (9)}$$

$$\begin{aligned}\Delta\bar{G}_{\mathrm{Al}}^{\mathrm{ex}} &= RT\ln\gamma_{\mathrm{Al}}\\ &= \Delta G^{\mathrm{ex}} - X_{\mathrm{Co}}\frac{\partial\Delta G^{\mathrm{ex}}}{\partial X_{\mathrm{Co}}} + \left(1-X_{\mathrm{Al}}\right)\frac{\partial\Delta G^{\mathrm{ex}}}{\partial X_{\mathrm{Al}}} - X_{\mathrm{O}}\frac{\partial\Delta G^{\mathrm{ex}}}{\partial X_{\mathrm{O}}}\\ &= -X_{\mathrm{Fe}}X_{\mathrm{Co}}{}^{0}\Omega_{\mathrm{Fe-Co}} - 2X_{\mathrm{Fe}}X_{\mathrm{Co}}\left(X_{\mathrm{Fe}}-X_{\mathrm{Co}}\right){}^{1}\Omega_{\mathrm{Fe-Co}}\\ &\quad - 3X_{\mathrm{Fe}}X_{\mathrm{Co}}\left(X_{Fe}^2-2X_{\mathrm{Fe}}X_{\mathrm{Co}}+X_{Co}^2\right){}^{2}\Omega_{\mathrm{Fe-Co}}\\ &\quad + X_{\mathrm{Fe}}\left(1-X_{\mathrm{Al}}\right){}^{0}\Omega_{\mathrm{Fe-Al}}\\ &\quad + X_{\mathrm{Fe}}\left(X_{\mathrm{Fe}}-2X_{\mathrm{Al}}-2X_{\mathrm{Fe}}X_{\mathrm{Al}}+2X_{\mathrm{Al}}^2\right){}^{1}\Omega_{\mathrm{Fe-Al}}\\ &\quad - X_{\mathrm{Fe}}X_{\mathrm{O}}{}^{0}\Omega_{\mathrm{Fe-O}} - 2X_{\mathrm{Fe}}X_{\mathrm{O}}\left(X_{\mathrm{Fe}}-X_{\mathrm{O}}\right){}^{1}\Omega_{\mathrm{Fe-O}}\\ &\quad + X_{\mathrm{Co}}\left(1-X_{\mathrm{Al}}\right){}^{0}\Omega_{\mathrm{Co-Al}}\\ &\quad + X_{\mathrm{Co}}\left(X_{\mathrm{Co}}-2X_{\mathrm{Al}}-2X_{\mathrm{Co}}X_{\mathrm{Al}}+2X_{\mathrm{Al}}^2\right){}^{1}\Omega_{\mathrm{Co-Al}}\\ &\quad - X_{\mathrm{Co}}X_{\mathrm{O}}{}^{0}\Omega_{\mathrm{Co-O}} - 2X_{\mathrm{Co}}X_{\mathrm{O}}\left(X_{\mathrm{Co}}-X_{\mathrm{O}}\right){}^{1}\Omega_{\mathrm{Co-O}}\\ &\quad + X_{\mathrm{O}}\left(1-X_{\mathrm{Al}}\right){}^{0}\Omega_{\mathrm{Al-O}}\end{aligned} \quad \text{..... (10)}$$

$$\begin{aligned}\Delta\bar{G}_{\mathrm{O}}^{\mathrm{ex}} &= RT\ln\gamma_{\mathrm{O}}\\ &= \Delta G^{\mathrm{ex}} - X_{\mathrm{Co}}\frac{\partial\Delta G^{\mathrm{ex}}}{\partial X_{\mathrm{Co}}} - X_{\mathrm{Al}}\frac{\partial\Delta G^{\mathrm{ex}}}{\partial X_{\mathrm{Al}}} + \left(1-X_{\mathrm{O}}\right)\frac{\partial\Delta G^{\mathrm{ex}}}{\partial X_{\mathrm{O}}}\\ &= -X_{\mathrm{Fe}}X_{\mathrm{Co}}{}^{0}\Omega_{\mathrm{Fe-Co}} - 2X_{\mathrm{Fe}}X_{\mathrm{Co}}\left(X_{\mathrm{Fe}}-X_{\mathrm{Co}}\right){}^{1}\Omega_{\mathrm{Fe-Co}}\\ &\quad - 3X_{\mathrm{Fe}}X_{\mathrm{Co}}\left(X_{Fe}^2-2X_{\mathrm{Fe}}X_{\mathrm{Co}}+X_{Co}^2\right){}^{2}\Omega_{\mathrm{Fe-Co}}\\ &\quad - X_{\mathrm{Fe}}X_{\mathrm{Al}}{}^{0}\Omega_{\mathrm{Fe-Al}} - 2X_{\mathrm{Fe}}X_{\mathrm{Al}}\left(X_{\mathrm{Fe}}-X_{\mathrm{Al}}\right){}^{1}\Omega_{\mathrm{Fe-Al}}\\ &\quad + X_{\mathrm{Fe}}\left(1-X_{\mathrm{O}}\right){}^{0}\Omega_{\mathrm{Fe-O}}\\ &\quad + X_{\mathrm{Fe}}\left(X_{\mathrm{Fe}}-2X_{\mathrm{O}}-2X_{\mathrm{Fe}}X_{\mathrm{O}}+2X_{\mathrm{O}}^2\right){}^{1}\Omega_{\mathrm{Fe-O}}\\ &\quad - X_{\mathrm{Co}}X_{\mathrm{Al}}{}^{0}\Omega_{\mathrm{Co-Al}} - 2X_{\mathrm{Co}}X_{\mathrm{Al}}\left(X_{\mathrm{Co}}-X_{\mathrm{Al}}\right){}^{1}\Omega_{\mathrm{Co-Al}}\\ &\quad + X_{\mathrm{Co}}\left(1-X_{\mathrm{O}}\right){}^{0}\Omega_{\mathrm{Co-O}}\\ &\quad + X_{\mathrm{Co}}\left(X_{\mathrm{Co}}-2X_{\mathrm{O}}-2X_{\mathrm{Co}}X_{\mathrm{O}}+2X_{\mathrm{O}}^2\right){}^{1}\Omega_{\mathrm{Co-O}}\\ &\quad + X_{\mathrm{Al}}\left(1-X_{\mathrm{O}}\right){}^{0}\Omega_{\mathrm{Al-O}}\end{aligned} \quad \text{..... (11)}$$

Finally, by substituting Eqs. (10) and (11) into Eq. (7), the fundamental equation for the numerical analysis of Al-deoxidation in molten Fe–Co alloy in equilibrium with Al_2O_3 can be obtained as follows.

$$\begin{aligned}&-5X_{\mathrm{Fe}}X_{\mathrm{Co}}{}^{0}\Omega_{\mathrm{Fe-Co}} - 10X_{\mathrm{Fe}}X_{\mathrm{Co}}\left(X_{\mathrm{Fe}}-X_{\mathrm{Co}}\right){}^{1}\Omega_{\mathrm{Fe-Co}}\\ &-15X_{\mathrm{Fe}}X_{\mathrm{Co}}\left(X_{Fe}^2-2X_{\mathrm{Fe}}X_{\mathrm{Co}}+X_{Co}^2\right){}^{2}\Omega_{\mathrm{Fe-Co}}\\ &+X_{\mathrm{Fe}}\left(2-5X_{\mathrm{Al}}\right){}^{0}\Omega_{\mathrm{Fe-Al}}\\ &+2X_{\mathrm{Fe}}\left(X_{\mathrm{Fe}}-2X_{\mathrm{Al}}-5X_{\mathrm{Fe}}X_{\mathrm{Al}}+5X_{\mathrm{Al}}^2\right){}^{1}\Omega_{\mathrm{Fe-Al}}\\ &+X_{\mathrm{Fe}}\left(3-5X_{\mathrm{O}}\right){}^{0}\Omega_{\mathrm{Fe-O}}\\ &+X_{\mathrm{Fe}}\left(3X_{\mathrm{Fe}}-6X_{\mathrm{O}}-10X_{\mathrm{Fe}}X_{\mathrm{O}}+10X_{\mathrm{O}}^2\right){}^{1}\Omega_{\mathrm{Fe-O}}\\ &+X_{\mathrm{Co}}\left(2-5X_{\mathrm{Al}}\right){}^{0}\Omega_{\mathrm{Co-Al}}\\ &+2X_{\mathrm{Co}}\left(X_{\mathrm{Co}}-2X_{\mathrm{Al}}-5X_{\mathrm{Co}}X_{\mathrm{Al}}+5X_{\mathrm{Al}}^2\right){}^{1}\Omega_{\mathrm{Co-Al}}\\ &+X_{\mathrm{Co}}\left(3-5X_{\mathrm{O}}\right){}^{0}\Omega_{\mathrm{Co-O}}\\ &+X_{\mathrm{Co}}\left(3X_{\mathrm{Co}}-6X_{\mathrm{O}}-10X_{\mathrm{Co}}X_{\mathrm{O}}+10X_{\mathrm{O}}^2\right){}^{1}\Omega_{\mathrm{Co-O}}\\ &+\left(3X_{\mathrm{Al}}+2X_{\mathrm{O}}-5X_{\mathrm{Al}}X_{\mathrm{O}}\right){}^{0}\Omega_{\mathrm{Al-O}}\\ &+2RT\ln X_{\mathrm{Al}} + 3RT\ln X_{\mathrm{O}} - \Delta G_{f,Al_2O_3}^{\circ} = 0\end{aligned} \quad \text{..... (12)}$$

The available binary interaction parameters from literature are summarized in **Table 2**. Meanwhile, the Gibbs free energy of formation of Al_2O_3 was taken from the NIST-JANAF Thermochemical Tables. Next, by further rearranging the above equation, the following relationship can be obtained such that the known binary interaction parameters are on the left-hand side of the equation and the unknown binary interaction parameters are on the right-hand side of the equation.

Table 2. List of binary interaction parameters used in this study.

		Value [J/mol]	Reference
Fe–Co	Ω^0_{Fe-Co}	9 939 − 3.29 T	22)
	Ω^1_{Fe-Co}	1 713 − 0.91 T	
	Ω^2_{Fe-Co}	−1 271	
Fe–O	Ω^0_{Fe-O}	−41 500 + 142.4 T	10)
	Ω^1_{Fe-O}	298 300 − 117.8 T	
Fe–Al	Ω^0_{Fe-Al}	−275 700 + 106.9 T	10)
	Ω^1_{Fe-Al}	79 940 − 35.85 T	
Co–O	Ω^0_{Co-O}	−92 260 + 10.35 T	18)
	Ω^1_{Co-O}	30 750 − 3.45 T	
Co–Al	Ω^0_{Co-Al}	−387 360	Present Study
	Ω^1_{Co-Al}	309 420	
Al–O	Ω^0_{Al-O}	856 300 − 1 497 T	10)
	$\Delta G^\circ_{Al_2O_3}$	−1 682 300 + 324.15 T	23)

$$
\begin{aligned}
Y_{Co(Al)} = \Big[& 5X_{Fe}X_{Co}\,{}^0\Omega_{Fe-Co} + 10X_{Fe}X_{Co}\left(X_{Fe}-X_{Co}\right){}^1\Omega_{Fe-Co} \\
& + 15X_{Fe}X_{Co}\left(X_{Fe}^2 - 2X_{Fe}X_{Co} + X_{Co}^2\right){}^2\Omega_{Fe-Co} \\
& - X_{Fe}\left(2-5X_{Al}\right){}^0\Omega_{Fe-Al} \\
& - 2X_{Fe}\left(X_{Fe} - 2X_{Al} - 5X_{Fe}X_{Al} + 5X_{Al}^2\right){}^1\Omega_{Fe-Al} \\
& - X_{Fe}\left(3-5X_O\right){}^0\Omega_{Fe-O} \\
& - X_{Fe}\left(3X_{Fe} - 6X_O - 10X_{Fe}X_O + 10X_O^2\right){}^1\Omega_{Fe-O} \\
& - X_{Co}\left(3-5X_O\right){}^0\Omega_{Co-O} \\
& - X_{Co}\left(3X_{Co} - 6X_O - 10X_{Co}X_O + 10X_O^2\right){}^1\Omega_{Co-O} \\
& - \left(3X_{Al} + 2X_O - 5X_{Al}X_O\right){}^0\Omega_{Al-O} \\
& - 2RT\ln X_{Al} - 3RT\ln X_O + \Delta G^\circ_{f,Al_2O_3}\Big] / X_{Co}\left(2-5X_{Al}\right) \\
= {}^0\Omega_{Co-Al} & + \frac{2\left(X_{Co} - 2X_{Al} - 5X_{Co}X_{Al} + 5X_{Al}^2\right)}{2-5X_{Al}}\,{}^1\Omega_{Co-Al}
\end{aligned}
\quad \cdots\cdots (13)
$$

By fitting the present experimental data taking $Y_{Co(Al)}$ as the vertical axis and $2(X_{Co}-2X_{Al}-5X_{Co}X_{Al}+5X_{Al}^2)/(2-5X_{Al})$ as the horizontal axis, the unknown binary interaction parameters, ${}^0\Omega_{Co-Al}$ and ${}^1\Omega_{Co-Al}$, in the right-hand side of the equation can be determined from the intercept and the slope of the regressed line, respectively. **Figure 2** shows the regressed line at 1 873 K such that the following values are obtained.

$$
{}^0\Omega_{Co-Al} = -387\,360\ [\text{J/mol}] \quad \cdots\cdots (14)
$$

$$
{}^1\Omega_{Co-Al} = 309\,420\ [\text{J/mol}] \quad \cdots\cdots (15)
$$

Using these values, it is now possible to express the Al-deoxidation equilibrium in molten Fe–Co alloy and pure liquid cobalt with Al_2O_3. The calculated Al–O equilibrium relationship in molten Fe–Co alloy at 1 873 K is shown in **Fig. 3** with the present experimental data. The apparent

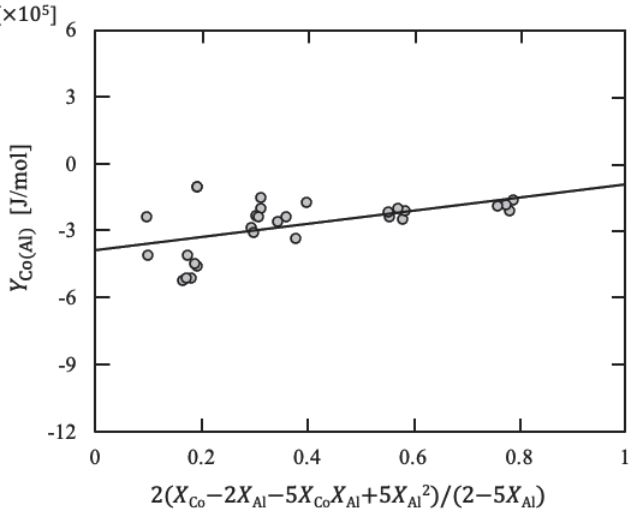

Fig. 2. Determination of ${}^0\Omega_{Co-Al}$ and ${}^1\Omega_{Co-Al}$ from the experimental values at 1 873 K.

deoxidation product of aluminum in molten Fe–Co alloy derived from the present work is also shown in **Fig. 4** with the current experimental data. Initially, the degree of deoxidation using aluminum was found to decrease with increasing cobalt concentration in the alloy, peaking at around 40 to 60 mass% Co, and then improved with further increase in cobalt concentration. In addition, Al-deoxidation efficiency was found to be low at high aluminum concentrations of about 0.5 mass% Al, and increased greatly at aluminum concentrations of about 0.1 mass% Al. However, further decrease in aluminum concentration to about 0.02 mass% Al was found to have little effect on the degree of deoxidation. These results suggest that for Fe-30 mass% Co to Fe-80 mass% Co, simple Al-deoxidation is not enough to sufficiently reduce oxygen concentration and hence complex deoxidation may be necessary.

In addition, utilizing the derived binary interaction parameters ${}^0\Omega_{Co-Al}$ and ${}^1\Omega_{Co-Al}$, and substituting $X_{Fe} = 0$ into Eq. (12), the Al–O equilibrium relationship in pure liquid cobalt was calculated and compared with the reported values by Ishihara *et al.* at 1 873 K in **Fig. 5**.[12] It was found that using the binary interaction parameters obtained in the present numerical assessment, Al-deoxidation equilibrium in pure liquid cobalt can also be accurately determined. Therefore, using the results from this study, Al-deoxidation equilibrium in molten Fe–Co alloy and in pure liquid cobalt can be quantitively expressed with a high level of accuracy, which is of huge importance in the production of high-quality Fe–Co based magnetic and structural materials.

3.3. Al-deoxidation in Equilibrium with $CoO{\cdot}Al_2O_3$

As mentioned in the preceding section, the oxide phase in equilibrium with molten Fe–Co alloy was Al_2O_3 for almost all samples. However, in the case of Sample 26 containing 80 mass% Co, it was found that $CoO{\cdot}Al_2O_3$ formed as the equilibrium phase. SEM-EDS mapping of the metal and crucible interface is shown in **Fig. 6** and it was found by point analysis that the aluminum to cobalt molar ratio was approximately Al:Co = 2:1, confirming the formation of $CoO{\cdot}Al_2O_3$. In this case, since $CoO{\cdot}Al_2O_3$ formed instead of Al_2O_3, the equilibrium deoxidation reaction changes to

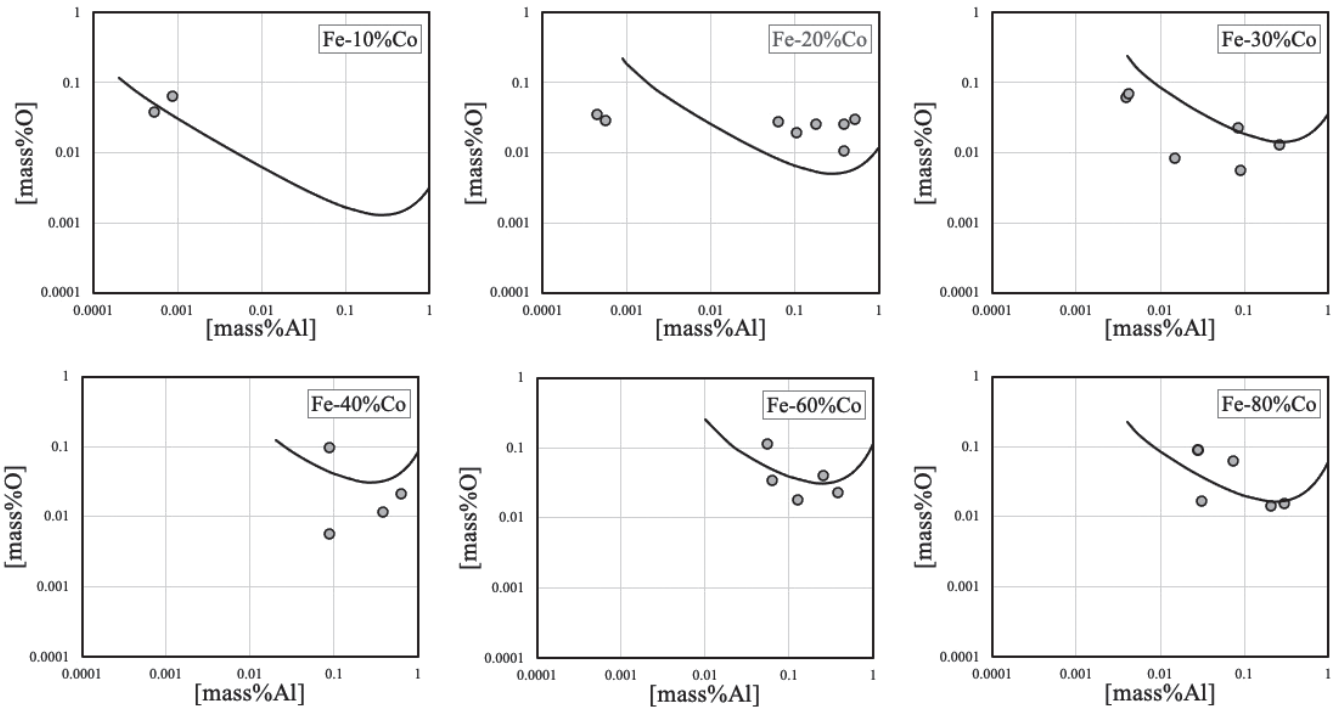

Fig. 3. Al–O equilibrium relationship in Al-deoxidized molten Fe–Co alloy at 1 873 K.

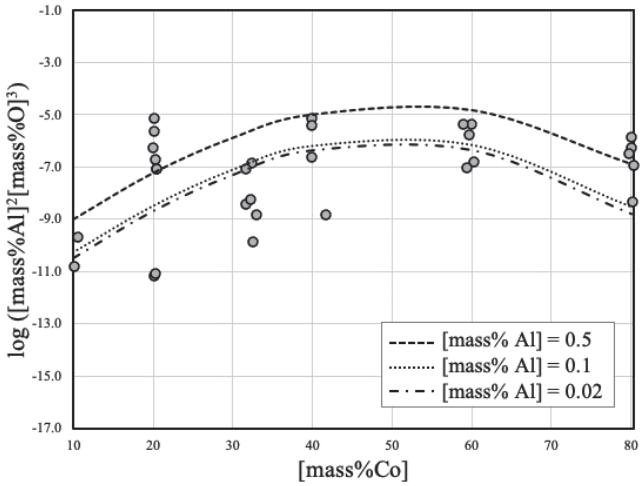

Fig. 4. Relationship between Co concentration and Al–O solubility product at 1 873 K.

the following equation:

$$\mathrm{Co}(\mathrm{l})+2[\mathrm{Al}]+4[\mathrm{O}]=\mathrm{CoO}\cdot\mathrm{Al_2O_3}(\mathrm{s}) \quad \text{..... (16)}$$

And the equilibrium constant, $K_{CoO\cdot Al_2O_3}$, of the above equation can then be expressed as follows where $\Delta G^{\circ}_{f,CoO\cdot Al_2O_3}$ is the Gibbs free energy of formation of $CoO\cdot Al_2O_3$. Since the dissolution of FeO in the generated oxide was found to be negligible from SEM-EDS point analysis, the activity of $CoO\cdot Al_2O_3$ can be assumed as unity.

$$\begin{aligned}\ln K_{\mathrm{CoO\cdot Al_2O_3}} &= -\frac{\Delta G^{\circ}_{f,CoO\cdot Al_2O_3}}{RT}\\ &= \ln a_{\mathrm{CoO\cdot Al_2O_3}} - \ln\gamma_{\mathrm{Co}} - 2\ln\gamma_{\mathrm{Al}} - 4\ln\gamma_{\mathrm{O}}\\ &\quad -\ln X_{\mathrm{Co}} - 2\ln X_{\mathrm{Al}} - 4\ln X_{\mathrm{O}} \qquad \text{..... (17)}\\ &= -\ln\gamma_{\mathrm{Co}} - 2\ln\gamma_{\mathrm{Al}} - 4\ln\gamma_{\mathrm{O}}\\ &\quad -\ln X_{\mathrm{Co}} - 2\ln X_{\mathrm{Al}} - 4\ln X_{\mathrm{O}}\\ &\quad (\therefore a_{CoO\cdot Al_2O_3}=1)\end{aligned}$$

Then, by utilizing the same assessment method earlier and by substituting Eqs. (9), (10) and (11) into the above equation, the following relationship is obtained.

$$\begin{aligned}&X_{\mathrm{Fe}}(1-7X_{\mathrm{Fe}})^{0}\Omega_{\mathrm{Fe-Co}}\\ &+X_{\mathrm{Fe}}\left(X_{\mathrm{Fe}}-2X_{\mathrm{Co}}-14X_{\mathrm{Fe}}X_{\mathrm{Co}}+14X_{\mathrm{Co}}^2\right)^{1}\Omega_{\mathrm{Fe-Co}}\\ &+X_{\mathrm{Fe}}\left(X_{\mathrm{Fe}}^2+3X_{\mathrm{Co}}^2-4X_{\mathrm{Fe}}X_{\mathrm{Co}}-21X_{\mathrm{Fe}}^2X_{\mathrm{Co}}\right.\\ &\left.+42X_{\mathrm{Fe}}X_{\mathrm{Co}}^2-21X_{\mathrm{Co}}^3\right)^{2}\Omega_{\mathrm{Fe-Co}}\\ &+X_{\mathrm{Fe}}(2-7X_{\mathrm{Al}})^{0}\Omega_{\mathrm{Fe-Al}}\\ &+2X_{\mathrm{Fe}}\left(X_{\mathrm{Fe}}-2X_{\mathrm{Al}}-7X_{\mathrm{Fe}}X_{\mathrm{Al}}+7X_{\mathrm{Al}}^2\right)^{1}\Omega_{\mathrm{Fe-Al}}\\ &+X_{\mathrm{Fe}}(4-7X_{\mathrm{O}})^{0}\Omega_{\mathrm{Fe-O}}\\ &+2X_{\mathrm{Fe}}\left(2X_{\mathrm{Fe}}-4X_{\mathrm{O}}-7X_{\mathrm{Fe}}X_{\mathrm{O}}+7X_{\mathrm{O}}^2\right)^{1}\Omega_{\mathrm{Fe-O}}\\ &+(2X_{\mathrm{Co}}+X_{\mathrm{Al}}-7X_{\mathrm{Co}}X_{\mathrm{Al}})^{0}\Omega_{\mathrm{Co-Al}}\\ &+\left(2X_{\mathrm{Co}}^2-X_{\mathrm{Al}}^2-2X_{\mathrm{Co}}X_{\mathrm{Al}}-14X_{\mathrm{Co}}^2X_{\mathrm{Al}}+14X_{\mathrm{Co}}X_{\mathrm{Al}}^2\right)^{1}\Omega_{\mathrm{Co-Al}}\\ &+(4X_{\mathrm{Co}}+X_{\mathrm{O}}-7X_{\mathrm{Co}}X_{\mathrm{O}})^{0}\Omega_{\mathrm{Co-O}}\\ &+\left(4X_{\mathrm{Co}}^2-X_{\mathrm{O}}^2-6X_{\mathrm{Co}}X_{\mathrm{O}}-14X_{\mathrm{Co}}^2X_{\mathrm{O}}+14X_{\mathrm{Co}}X_{\mathrm{O}}^2\right)^{1}\Omega_{\mathrm{Co-O}}\\ &+(4X_{\mathrm{Al}}+2X_{\mathrm{O}}-7X_{\mathrm{Al}}X_{\mathrm{O}})^{0}\Omega_{\mathrm{Al-O}}\\ &+RT\ln X_{\mathrm{Co}}+2RT\ln X_{\mathrm{Al}}+4RT\ln X_{\mathrm{O}}-\Delta G^{\circ}_{f,CoO\cdot Al_2O_3}=0\end{aligned}$$

..... (18)

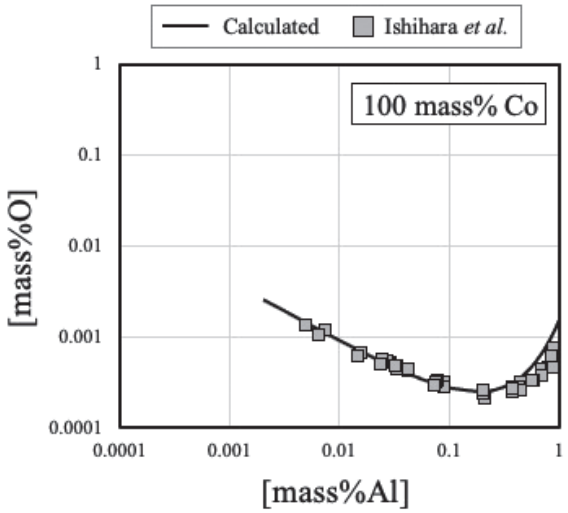

Fig. 5. Al–O equilibrium relationship in pure liquid cobalt metal at 1 873 K.

The above equation becomes the fundamental equation for the numerical analysis of Al-deoxidation in molten Fe–Co alloy in equilibrium with $CoO{\cdot}Al_2O_3$. Next, using the experimental results of the Al-deoxidation experiment in Fe-80 mass% Co alloy, it is possible to estimate the critical point where Al_2O_3 and $CoO{\cdot}Al_2O_3$ coexist at 1 873 K. As listed in Table 1, the equilibrium phase in Sample 27 was Al_2O_3 whereas that with Sample 26 was $CoO{\cdot}Al_2O_3$, such that the critical point should be in between the range of $0.029 < [\text{mass\% Al}] < 0.031$ and $0.086 < [\text{mass\% O}] < 0.0167$. Using Eq. (18), the value of the Gibbs free energy of formation of $CoO{\cdot}Al_2O_3$ that satisfies this range should therefore be between −1 268 to −1 269 kJ/mol. By combining the reported values of Aleksandrov *et al.* and Hino *et al.*, the Gibbs free energy of $CoO{\cdot}Al_2O_3$ formation can be estimated as -1 203 kJ/mol, which more or less agrees with the experimentally obtained value.[2,10]

From the fundamental equations for the Al-deoxidation in

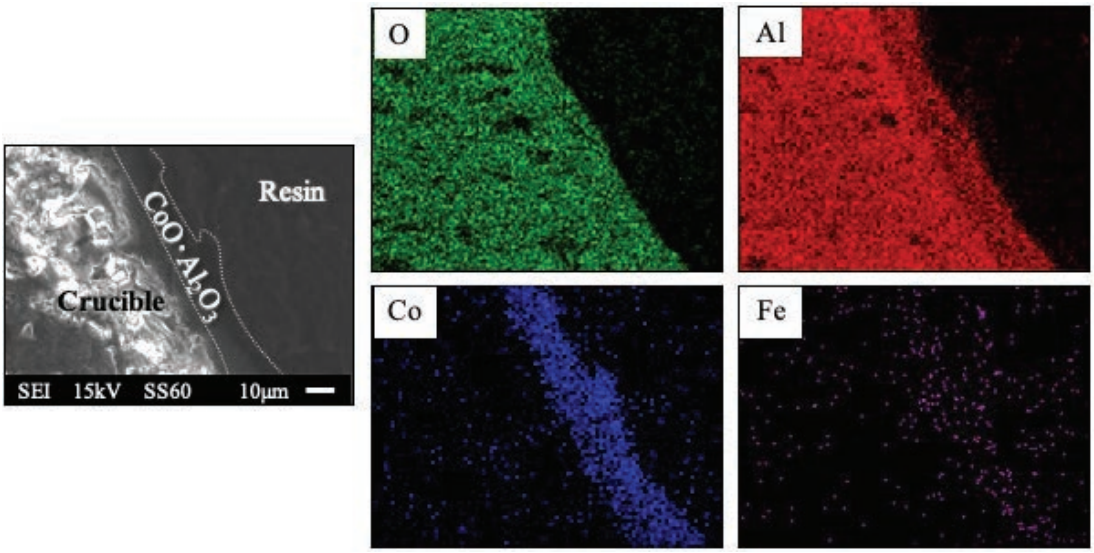

Fig. 6. Elemental mapping of the metal and crucible interface indicating the formation of cobalt aluminate ($CoO{\cdot}Al_2O_3$). (Online version in color.)

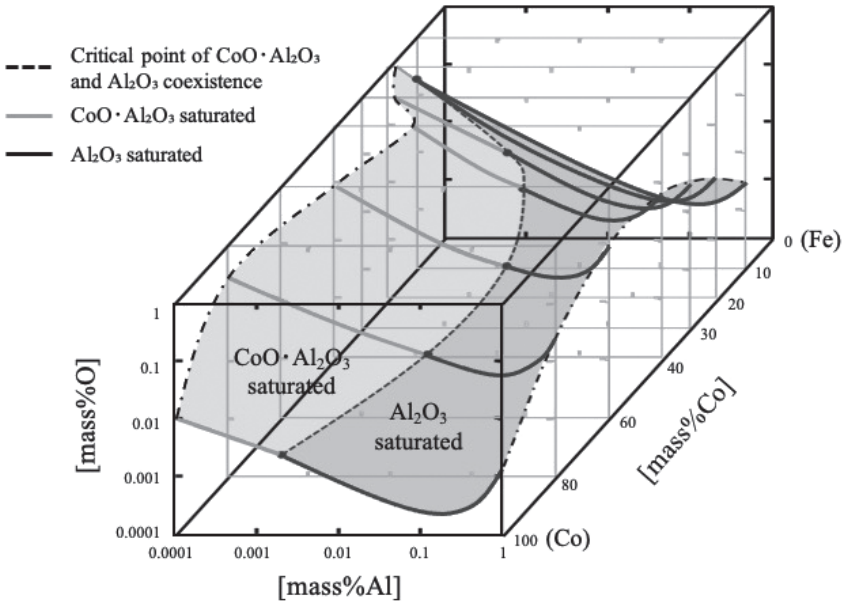

Fig. 7. Al–O relationship in molten Fe–Co alloy saturated with Al_2O_3 or $CoO{\cdot}Al_2O_3$ at 1 873 K.

molten Fe–Co alloy, Eqs. (12) and (18), the Al–O relation in equilibrium with Al_2O_3 and $CoO{\cdot}Al_2O_3$ at 1 873 K can be estimated as shown in **Fig. 7**. The critical point that Al_2O_3 and $CoO{\cdot}Al_2O_3$ coexist was found to shift to higher Al content with increasing Co concentration in the alloy until the maximum at around 40 to 60 mass% Co. In addition, experimental results of Ishihara *et al.* under Al_2O_3 saturated conditions shown in Fig. 5 corresponds well with the position of the calculated critical point in pure liquid cobalt, further validating the accuracy of the current assessment.[12] In the case of maraging steels with about 10 mass% Co, it was found that oxygen concentration can be sufficiently reduced to about 13 ppm, which is great importance in view of producing defect-free structural materials.

4. Conclusions

Aluminum deoxidation equilibrium in molten Fe–Co alloys and pure liquid cobalt at 1 873 K was investigated in this study. Using the present experimental data, Al–O equilibrium relationship was quantitively expressed using binary interaction parameters derived on the basis of the quadratic formalism and Redlich-Kister type polynomial. Moreover, using the experimental data in Fe-80 mass% Co sample, the critical point at which Al_2O_3 and $CoO{\cdot}Al_2O_3$ coexist was determined and the Gibbs free energy of $CoO{\cdot}Al_2O_3$ was estimated. It was found that sufficiently low oxygen values can be achieved in Fe-10 mass Co alloys, which is the typical composition of maraging steels. However, for alloys with higher cobalt concentrations (40 to 60 mass% Co), simple Al-deoxidation cannot sufficiently reduce oxygen concentration and hence complex deoxidation may be necessary. Finally, the critical aluminum and oxygen concentrations wherein Al_2O_3 and $CoO{\cdot}Al_2O_3$ coexist was found to shift to higher Al content until the maximum at around 60 mass% Co.

REFERENCES

1) A. A. Couto and P. I. Ferreira: *J. Mater. Eng.*, **11** (1989), 31.
2) A. A. Aleksandrov and V. Ya. Dashevskii: *Russ. Metall.*, **2014** (2014), 185.
3) J. Katsuki and T. Yamauchi: *CAMP-ISIJ*, **7** (1994), 1076.
4) S.-W. Cho and H. Suito: *Steel Res.*, **66** (1995), 237.
5) G. Li, R. Inoue and H. Suito: *Steel Res.*, **67** (1996), 528.
6) F. Ishii, S. Ban-ya and M. Hino: *ISIJ Int.*, **36** (1996), 25.
7) H. Fujiwara, A. Hattori and E. Ichise: *Tetsu-to-Hagané*, **85** (1999), 201 (in Japanese).
8) S.-B. Lee, S.-M. Jung, H.-G. Lee and C.-H. Rhee: *ISIJ Int.*, **42** (2002), 679.
9) H. Ohta and H. Suito: *ISIJ Int.*, **43** (2003), 1301.
10) A. Hayashi, T. Uenishi, H. Kandori, T. Miki and M. Hino: *ISIJ Int.*, **48** (2008), 1533.
11) H. Fukaya, K. Kajikawa, A. Malfliet, B. Blanpain and M. Guo: *Metall. Mater. Trans. B*, **49** (2018), 2389.
12) I. Ishihara, K. Takahashi, M. Kawaguchi, F. Ishii and M. Hino: *J. Jpn. Inst. Met.*, **61** (1997), 1064.
13) L. S. Darken: *Trans. Metall. Soc. AIME*, **239** (1967), 80.
14) M. Hillert and L.-I. Staffansson: *Acta Chem. Scand.*, **24** (1970), 3618.
15) N. Saunders and A. P. Miodownik: Calphad, A Comprehensive Guide, Pergamon, Oxford, UK, (1988), 91.
16) T. Miki, F. Ishii and M. Hino: *Mater. Trans.*, **44** (2003), 1817.
17) T. Miki and M. Hino: *ISIJ Int.*, **44** (2004), 1800.
18) T. Miki and M. Hino: *ISIJ Int.*, **45** (2005), 1848.
19) W. Y. Cha, T. Nagasaka, T. Miki, Y. Sasaki and M. Hino: *ISIJ Int.*, **46** (2006), 996.
20) T. Miki, K. Tsujita, S. Ban-ya and M. Hino: *Calphad*, **30** (2006), 449.
21) H. Okamoto: *J. Phase Equilib. Diffus.*, **29** (2008), 383.
22) J. Wang, X. G. Lu, N. Zhu and W. Zheng: *Calphad*, **58** (2017), 82.
23) M. W. Chase, Jr., ed.: NIST-JANAF Thermochemical Tables, 4th ed., *J. Phys. Chem. Ref. Data*, American Institute of Physics, Woodbury, NY, (1998), 154.